

This is the peer reviewed version of the following article: Cánovas-García, F., Pesántez-Cobos, P. & Alonso-Sarría, F. (2020). fusionImage: An R package for pan-sharpening images in open source software. *Transactions in GIS*, 24(5), 1185–1207. which has been published in final form at: <https://doi.org/10.1111/tgis.12676>

This article may be used for non-commercial purposes in accordance with Wiley Terms and Conditions for Use of Self-Archived Versions. This article may not be enhanced, enriched or otherwise transformed into a derivative work, without express permission from Wiley or by statutory rights under applicable legislation. Copyright notices must not be removed, obscured or modified. The article must be linked to Wiley's version of record on Wiley Online Library and any embedding, framing or otherwise making available the article or pages thereof by third parties from platforms, services and websites other than Wiley Online Library must be prohibited.

fusionImage: An R package for pan-sharpening images in open source software

Fulgencio Cánovas-García^{1,2,3*} | Paúl Pesántez-Cobos^{4*}

| Francisco Alonso-Sarría^{5*}

¹Departamento de Geografía Humana, Universidad de Sevilla, María de Padilla, s/n. 41004 Sevilla, Spain

²Universidad Técnica Particular de Loja, Departamento de Geología y Minas e Ingeniería Civil, San Cayetano Alto S/N, Loja, Ecuador, 110107

³Departamento de Ingeniería Minera y Civil, Universidad Politécnica de Cartagena, Paseo Alfonso XIII, 52. 30203 Cartagena, Spain

⁴Universidad de Cuenca, Departamento de Ingeniería Civil, Av. 12 de abril. Ciudadela Universitaria, Cuenca, Ecuador

⁵Instituto Universitario del Agua y del Medio Ambiente, Universidad de Murcia. Edificio D, Campus de Espinardo, s/n, 30001 Murcia, Spain

Correspondence

Fulgencio Cánovas-García, Departamento de Geografía Humana, Universidad de Sevilla, María de Padilla, s/n. 41004 Sevilla, Spain
Email: fulgencio.canovas@um.es

Funding information

Saavedra Fajardo programme (Ref. 20023/SF/16) by the Fundación Séneca-Agencia de Ciencia y Tecnología de la Región de Murcia and the project CGL2017-84625-C2-2-R funded by the Spanish Ministry of Economy, Industry and Competitiveness (MINECO), the Spanish Research Agency (AEI) and European Regional Development Funds (FEDER).

* Equally contributing authors.

The objective of this paper is to evaluate the performance of three pan-sharpening algorithms (High Pass Filter, Principal Component Analysis and Gram-Schmidt) to increase the spatial resolution of five types of multispectral images and to evaluate the results in terms of color, coherence and spatial sharpness, both qualitatively and quantitatively. A secondary objective is to present an implementation of the aforementioned pan-sharpening techniques within the open source software R. From a qualitative point of view, pan-sharpening of images with a high spatial resolution ratio presents better results than of those whose spatial resolution ratio is two. According to the quantitative evaluation, there is no pan-sharpening methodology that obtains optimal results simultaneously for all types of images used. The results of the spectral and spatial index ERGAS vary for four out of the five types of images analysed. The results show that none of the methods implemented in this work can be considered a priori better than the others. At the same time, this work indicates the importance of both the qualitative and the quantitative assessment.

1 | INTRODUCTION

Image fusion has been described as a set of techniques that combines images of different spatial resolutions or containing different types of information with the objective of generating new images that enhance the properties of the originals (Liu and Mason, 2009). The overall aim is to improve data interpretability, either by improving their visual quality, by facilitating the discrimination of certain categories or by increasing the accuracy of subsequent analysis methods (Chuvieco, 2016). Pan-sharpening refers to the fusion of a panchromatic (PAN) and a multispectral (MS) image that are simultaneously acquired over the same area. This can be interpreted as a particular case of data fusion as the aim is to combine the spatial details in PAN with the spectral bands in the MS image into one product (Vivone et al., 2015). When a PAN band is available, light is collected for a wide range of wavelengths, usually covering all MS bands. This allows the pixel size to be reduced while still maintaining the minimum intensity necessary to trigger the PAN sensor (Brodu, 2017). Image pan-sharpening tries to minimise spatial and spectral distortion in the pan-sharpened images (Zhang and Roy, 2016).

The demand for pan-sharpened data is steadily rising due to the increasing availability of commercial products that provide high-resolution spatial imagery to the general public and users such as Google Earth and Bings Maps. In addition, pan-sharpening is a type of image preprocessing used for many remote sensing tasks such as change detection, object recognition or photointerpretation (Vivone et al., 2015). It is commonly used in both environmental and social sciences; for example, to improve the interpretation of geomorphological forms (Ewertowski et al., 2016) and the monitoring of urban sprawl (Huang et al., 2017). Another reason for image pan-sharpening is that more than 70 % of terrestrial observation satellites and a large number of digital aerial cameras are simultaneously equipped with PAN and MS sensors (Zhang, 2004; Zhang and Mishra, 2012). Landsat 8, GeoEye, OrbView, SPOT, WorldView and Pleiades are examples of this configuration, that enable users to take advantage of the complementarity of data sets coming from both types of sensors. The increasing number and availability of high-resolution optical satellites as well as the ever-improving revisit cycles, allow complementary high resolution and MS images to be obtained during the same season and possibly under similar atmospheric and illumination conditions (Yokoya et al., 2017). Snehmani et al. (2016) also state that pan-sharpening is one of the essential steps for improving the image quality of many remote sensing applications and that it is not obvious to non-specialists how to select one method in preference to the others for a given case.

The difference in spatial resolution between the PAN and the MS mode can be measured by the spatial resolution ratio (or spatial ratio), i.e. the ratio of their respective ground sampling distances. Spatial ratios usually vary between 2 and 5 (Ehlers et al., 2009, 2010), although the most common is a spatial ratio of 2 (LANDSAT ETM+ and OLI) or 4 (IKONOS-2, QuickBird-2, GeoEye-1/2, Pléiades and WorldView-2). This ratio may be even higher if data from different satellites are used (Klonus and Ehlers, 2009; Yokoya et al., 2017). Some studies have achieved acceptable results with ratios equal to or greater than four, depending on the image characteristics and the pan-sharpening methodology used (Zhang, 2002; Gangkofner et al., 2008; Yuhendra et al., 2010).

Several pan-sharpening algorithms have been proposed and some attempts have been made to classify them. A broader overview can be found in Pohl and Van Gendreen (1998) , Darvishi Bolorani (2008) , Amro et al. (2011) and Basaeed et al. (2013). Because of the differences that exist among sensors and among the Earth surface features, there is no consensus on which pan-sharpening technique provides the best results (Zhang and Roy, 2016). The way to effectively evaluate the quality of the results has been a challenge to researchers and users of these fused products. However, two approaches have been most widely used in research (Zhang, 2008):

- Qualitative approaches involve the visual comparison of the original MS and the fused images to verify colour

coherence, and a comparison of the original PAN and the pan-sharpened images to verify that spatial detail is preserved.

- Quantitative approaches involve a set of predefined quality indicators to measure the spectral and spatial similarities between the pan-sharpened and the original (PAN and MS) images.

R is an open source statistical programming environment (R Development Core Team, 2009) in which many of the new image processing developments are being implemented because of its power, flexibility, and community of developers and users, among other reasons. The use of R has increased, not only in statistics but also as a reference program in many scientific disciplines, including Geographic Information Systems and Remote Sensing with packages such as `raster` (Hijmans, 2016), `landsat` (Goslee, 2011) or `sf` (Pebesma, 2018). The `raster` package, in particular, has meant overcoming several limitations in the handling of large images. Pebesma et al. (2012) presents some arguments as to why R Software Environment is a good option for carrying out reproducible geoscientific research and Bivand et al. (2013) highlights the increasing importance of geospatial analysis in R usage and development.

The objective of this work were three-fold:

- To improve the spatial resolution of five images obtained using different technologies: QuickBird, IKONOS, Landsat 7, Landsat 8 and a Intergraph Z/I-Imaging Digital Mapping Camera.
- To implement in form of an open source program three pan-sharpening algorithms (High Pass Filter, Principal Component Analysis and Gram-Schmidt transformation) and two quality indices for the pan-sharpened images (spectral ERGAS -*erreur relative globale adimensionnelle de synthèse*- index, and ERGAS spatial index). Implementing the above mentioned algorithms as an open source is one of our research objectives since it facilitates transparency: open source software implies that all of the code within a given workflow is completely visible to the users. There are no hidden processes or black boxes (Hengl et al., 2018).
- To discuss the advantages and deficiencies of each pan-sharpening method in each of the study areas and sensors used.

2 | MATERIALS AND METHODS

2.1 | Analysed images

Figure 1 shows two maps identifying the locations which the images represent: one map with four images located between southern Ecuador and northern Peru (Figure 1 a) and the other with the image Natmur-08 in south-eastern Spain (Figure 1 b). The images were captured by sensors from five different platforms, and their main characteristics are shown in Table 1.

QuickBird was a commercial satellite launched on October 18, 2001, in an heliosynchronous orbit (450 km and 482 km altitude). It had two CCD cameras - one PAN and one MS (blue -B-, green -G-, red -R- and near infrared -NIR-bands). The sweeping width covered by these images was between 16.8 km and 18 km according to the orbital height (Digital Globe, 2013b). The satellite was deactivated in 2015, 2.5 years after its expected activity end date.

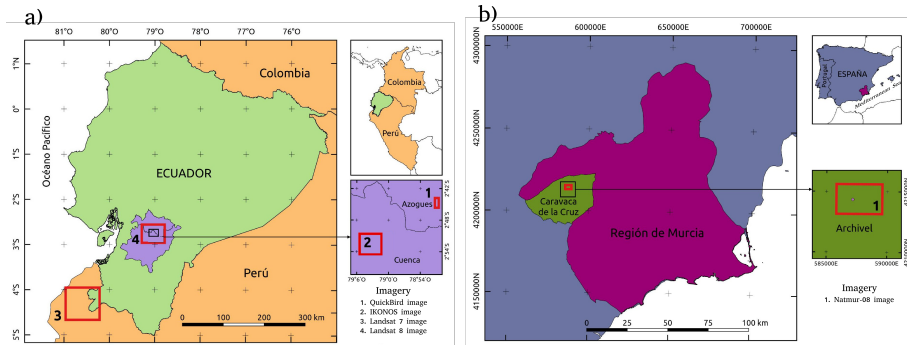
The analysed QuickBird image covers an area of 4.63 km² and corresponds to the city of Azogues (Ecuador), including part of the Burgay river which runs north-south. Several characteristic spots such as the Central Plaza, the Cuenca-Azogues highway, the bus station and the municipal stadium can be distinguished in the image. A subset of this is shown in Figure 2 a.

IKONOS was a commercial Earth observation satellite launched on September 24, 1999. It was the first satellite

TABLE 1 Main characteristics of the analysed images.

Platform	Spatial Res. (m)	Spectral Res.	Radiometric	Nº Rows	Nº Columns	EPSG
	MS, PAN	sensor, fused	Res. (bits)	(PAN)	(PAN)	code
QuickBird	2.4, 0.6	4, 4	11	5677	2267	32717
IKONOS	4, 1	4, 4	11	6109	5300	32717
Landsat 7	30, 15	7,4	8	5544	5823	32717
Landsat 8	30, 15	10,3	16	2977	3736	32617
Airbone sensor	2, 0.45	4, 4	12	5451	8401	25830

Res.: Resolution; EPSG: European Petroleum Survey Group.

**FIGURE 1** Location of the images used in this work. a) Ecuador-Peru and b) Spain.

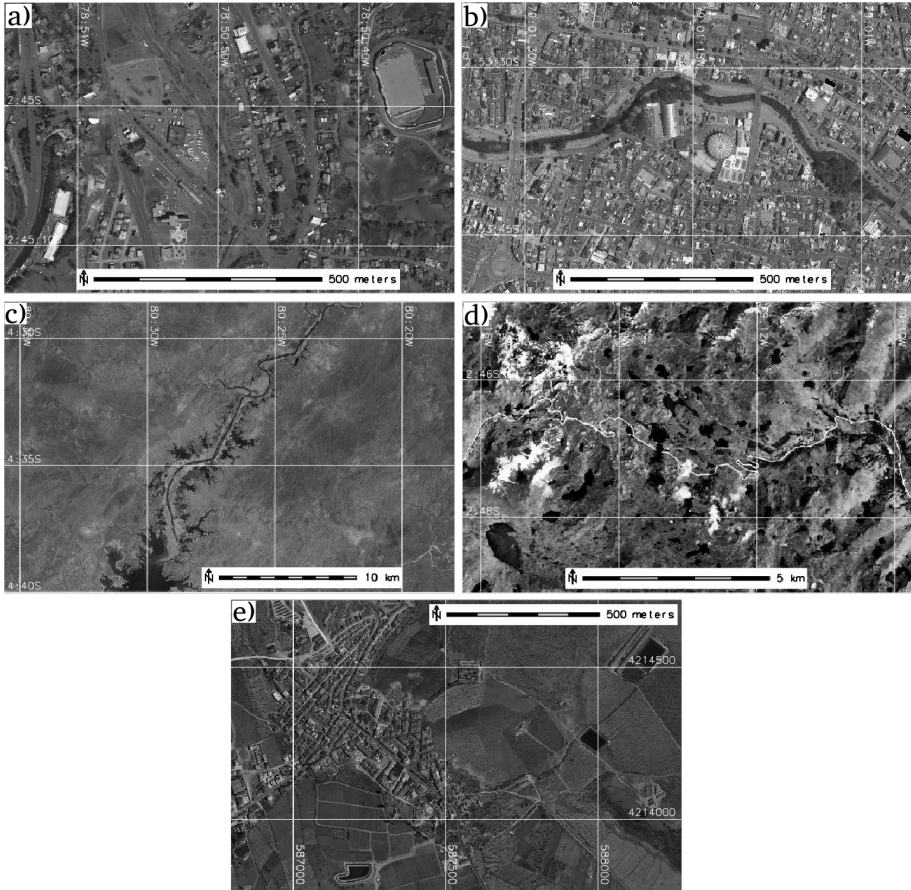


FIGURE 2 Zoom on the analysed images. (a) QuickBird; (b) IKONOS; (c) Landsat 7; (d) Landsat 8; (e) Natmur-08.

80 to make high-resolution images available to the public, constituting a milestone in remote sensing. In orbit at 681 km, the width of the images was 11 km (Digital Globe, 2013a). In January 2015, DigitalGlobe, the owner of the satellite, announced that, due to problems with quality standards, the satellite had been deactivated.

The analysed IKONOS image (32.4 km²) covers the western edge of the city of Cuenca and some small towns surrounding the city. Land use basically corresponds to buildings, crops, forests and shrubs. A subset of the panchromatic
85 image is shown in Figure 2 b.

Landsat 7 and 8 are part of a constellation of eight satellites that have provided Earth surface information since 1972. The Landsat project has been one of the most successful space remote sensing project developed to date (Chuvieco, 2016). The images used in this work were:

- Landsat 7 image corresponding to the continental part of image P011R063 acquired on October 25, 2001. It covers an area of 6555 km², and includes the south-western part of the Province of Loja (cantón Zapotillo, Ecuador) and part of the departments of Tumbes and Piura in Peru. There are no major urban centres such as provincial or departmental capitals. Most of the region is made up of dry forests, arid zones and small cultivated areas. This image distinguishes the Pozos Dam, which is part of the Chira-Piura Irrigation Project in Peru. A subset of the image is presented in Figure 2 c.
- Landsat 8 image (2502 km²) corresponding to a part of image P010R062 acquired on October 30, 2014. It covers the cities of Cuenca and Azogues, as well as the Cajas National Park. It is possible to distinguish a large area of the Andean *paramo* in the Ecuadorian Western Cordillera as well as urban zones, crops and forests. Figure 2 d shows a subset of the original PAN image.

The application of pan-sharpening algorithms near the Equator has been poorly documented in scientific work.
100 Almost all research on this subject uses images of places located at mid-latitudes. In low latitudes, the almost total absence of cloudless days, as it is located in the Intertropical Convergence Zone makes it difficult to obtain optical images, which was an added difficulty for carrying out this research.

The Natmur-08 project was a technical assistance programme carried out on behalf of the Murcia Regional Government (Region of Murcia, Spain), which consisted of taking digital photogrammetric images by airborne PAN and MS
105 (R, G, B, NIR bands) sensors (Intergraph Z/I-Imaging Digital Mapping Camera), and a LiDAR survey for the generation of digital terrain models. The project generated PAN images with a spatial resolution of 0.45 m and MS images with spatial resolutions of 2 m. The size of the image used was 5451 rows by 8401 columns (9.27 km²) and covers the hamlet of Archivel, belonging to the Municipality of Caravaca de la Cruz, in the Region of Murcia. A subset of the image is presented in Figure 2 e.

110 These images were chosen because they represent different combinations of terrestrial coverage and different sensors (four satellite-based platforms and one airborne). The resolution characteristics (spectral, spatial, radiometric) of the sensors made it possible to apply the three pan-sharpening techniques to images that represent, in our opinion, a wide range of the available resolutions. The spatial ratios of the images are shown in Table 2. This ratio is much higher for images of very high spatial resolution (QuickBird, IKONOS and Natmur-08) than for images of medium
115 spatial resolution (Landsat 7 and 8).

2.2 | Image pan-sharpening methods

Ideally, a good pan-sharpening method should not only increase the spatial resolution of MS data, but also preserve, as far as possible, its spectral integrity (Chavez et al., 1991; Laben and Brower, 2000; Ranchin and Wald, 2000). It

can be concluded from Liu and Mason (2009) that colour distortion can be significant if the spectral range of the MS bands is different from that of the PAN band. Taking these considerations into account, we have only performed pan-sharpening in the MS bands covered by the PAN and on those bands beyond the PAN that are highly correlated with the MS bands covered by the PAN. This is a somewhat less restrictive criterion than the used by Švab and Oštir (2006) who claim that the spectral bands used in pan-sharpening should cover the same wavelengths as the PAN band, and should follow a similar sensitivity to that of the sensor.

Three pan-sharpening algorithms are implemented: High Pass Filter, Principal Component Analysis and Gram-Schmidt transformation. The reasons for choosing them are that they produced appropriate results in previous studies and that they represent the main types of image pan-sharpening techniques (Karathanassi et al., 2007; Gangkofner et al., 2008; Yuhendra et al., 2010; Zhang and Mishra, 2012; Sarp, 2014; Cánovas-García and Alonso-Sarría, 2014). These algorithms are still used in recent pan-sharpening research and are still considered by several authors as state-of-the-art pan-sharpening methods (Snehmani et al., 2016; Vivone et al., 2015).

High Pass Filter (HPF), which counts among space domain image pan-sharpening techniques, inserts high frequency components into images of low spatial resolution. The HPF methodology was introduced by Schowengerdt (1980) as a data reconstruction and compression technique, and has been extended to new datasets to fuse images of different spatial and spectral resolutions (Chavez et al., 1984; Cliche et al., 1985; Chavez et al., 1991). According to Gangkofner et al. (2008), this technique has generally been implemented in a simplistic manner because the parameters used have not been optimised to achieve satisfactory spatial and radiometric results. The same author proposed an optimisation and standardisation of the method in order to guarantee its applicability to a wide range of images with different ratios between the MS and PAN spatial resolutions; (Gangkofner et al., 2008) the aforementioned standardisation method was applied in this research (see supplementary materials). Although the HPF algorithm implemented in this research dates back to 2008, it is still used with high spatial resolution images when pan-sharpening is used as an image preprocessing tool and the objective is land cover classification (Ghosh and Joshi, 2014).

Principal Components Analysis (PCA) is considered as a component replacement technique. It involves a linear transformation of the MS bands, the substitution of a variable in the transformed space, and inverse transformation to the original space (Shettigara, 1992). The justification for this substitution is that the PAN image is approximately equal to the first principal component, which contains information that is common to all the bands used as input in the PCA procedure, whereas the spectral information unique to each band is represented in the other components (Chavez et al., 1991). This substitution maximizes the effect of the high resolution PAN band on the fused bands resulting from the process (Shettigara, 1992). Although the PCA algorithm is one of the oldest and has been largely implemented in many commercial remote sensing packages, it is still used today with appropriate results when the objective is image classification (Gasparovic and Jogun, 2018) or in the restoration of pan-sharpened images (Duran and Buades, 2019).

Gram-Schmidt transformation, which is also considered a component substitution method (Aiazzi et al., 2006), was invented by Laben and Brower in 1998 and patented by Eastman Kodak (Laben and Brower, 2000). It is based on the Gram-Schmidt transformation, a vector orthogonalization process. In the case of images, each band corresponds to a high-dimensional vector (equal to the number of pixels in the image), which are rotated to produce a new set of uncorrelated vectors (Maurer, 2013). The algorithm is still used in specific pan-sharpening research. For example, Du et al. (2007) compared Brovey, GS, PCA, multiplicative method, and UBN pansharpening techniques on QuickBird and IKONOS images and concluded that Gram-Schmidt was among the methods that produced the best results. Karathanassi et al. (2007) compared IHS (Intensity, Hue and Saturation transformation), Brovey, PCA, GS, the local mean and variance matching (LMVM) and concluded that GS was one of the most efficient methods. Finally, Jawak and Luis (2013), after comparing six methods, concluded that GS produced the best results.

The GS pan-sharpening procedure, summarized in five steps, can be consulted in detail in Laben and Brower (2000) and in the supplementary materials of this article.

Our intention, therefore, was to use well known algorithms that have been well tested on a real application scale, without resorting to newer algorithms that have recently been shown to provide appropriate experimental results but which have hardly been used in remote sensing applications. In addition, our aim was to equate the functionalities that exist in free geospatial software with those in two of the most widely used proprietary remote sensing software today, such as ENVI and ERDAS Imagine (2013 versions).

Details of the R implementation of the three algorithms can be found in the supplementary materials.

2.3 | Image pan-sharpening assessment

Two evaluation approaches (qualitative and quantitative) were followed, both commonly used in pure and practical image pan-sharpening research (Belfiore et al., 2016; Kaplan, 2018; Pohl and Van Gendreen, 1998; Vivone et al., 2015).

There are no standard protocols for the visual evaluation of image pan-sharpening, although some criteria have been proposed (Wald et al., 1997; Lu et al., 1996; Shi et al., 2005; European Commission, 1997). This work takes into account spectral and spatial criteria. As spectral criteria we considered brightness, evaluating the perceptible intensity differences of a certain colour between the original and the fused image, and anomalous colours, taking into account variations of colour between both images. As regards spatial criteria, the fused image should maintain the sharpness of an object's outline and the spatial contrast between different elements without producing veined textures in the form of small elongated distortions that sometimes appear when a pan-sharpening algorithm is applied.

As the evaluation of the visual quality of merged images has a subjective component, it is important to ensure that the display conditions (monitor, histogram stretch, etc.) are consistent (Zhang, 2008). In any case, the bias and the experience of the evaluator will inevitably affect the evaluation (Wang et al., 2005; Ehlers and Astrand, 2008; Klonus and Ehlers, 2009; Fonseca et al., 2011; Jagalingam and Hegde, 2015). The thematic application must also be considered in relation to the aim of the fusion (Pellemans et al., 1993; Wald et al., 1997), which will condition the perception of the evaluator (Wald et al., 1997).

Ten mosaics (Figures 4 to 13), two for each sensor, containing a clip of the image in its original version, HPF pan-sharpened, PCA pan-sharpened and GS pan-sharpened were composed to perform the evaluation presented in Table 2. The clips selected were those with the most pronounced spectral contrast among the objects. For each case a colour composition was used to highlight these contrasts. When possible, the same colour composition was used for data obtained from the same sensor. Only when the contrast of the two images was not clear enough to recognise differences, did we use two different compositions for the data of the same sensor. To evaluate the mosaics, they were displayed with a linear adjustment of the histogram between the minimum and maximum percentiles (0.5 and 99.5 %, respectively) for all bands. A five level scale was used to assess the quality of the compositions: 1=very bad, 2=bad, 3=acceptable, 4=good, 5=very good. A qualitative assessment of the entire scene analysed was not considered feasible due to the time involved (as an example, about 350 similar clips to the IKONOS image would need to be analysed to cover the entire merged scene). In addition, the subjectivity of this type of validation could make the evaluation process unfeasible.

Pan-sharpening may cause alterations in the radiometry of the image that may be not visually perceivable, but enough to invalidate further analysis, such as atmospheric corrections or the estimation of variables. This is why, although necessary, visual assessment is not sufficient. An example of such alterations was described by Zhang (2008).

The quantitative evaluation was carried out using two algorithms: the spectral ERGAS index (or ERGAS index) and the spatial ERGAS index. We are aware that some researchers have used a high number of quality indices (Vivone

et al., 2015; Snehmani et al., 2016). However, without wishing to suggest that such an approach is not appropriate, we stress that the goal of the present research was to provide remote sensing practitioners with a powerful, but also rapid and efficient computational tool, for which reason we opted for the simplest quantitative evaluation possible.

The spectral ERGAS index proposed by Wald (2000) and Wald (2002), was used to compare the spectral quality of the pan-sharpened images. The three main requirements of this index are:

- Independence from the units, i.e., radiance values or quantities without units.
- Independence from the number of bands in the image to be pan-sharpened.
- Independence from the spatial resolution ratio between the MS and the PAN images.

To calculate this index in full resolution mode, the original MS bands are downsampled (DwMS) to the spatial resolution of the pan-sharpened bands (FMS or Fused Multi Spectral bands). We shall call this the *full resolution* analysis.

The *frERGAS* index (equation 2) uses the full resolution (*fr*) root mean square error (equation 1):

$$frRMSE = \sqrt{\frac{1}{P} \sum_{p=1}^P (DsMS_p - FMS_p)^2} \quad (1)$$

to measure the extent to which two bands differ, where p is each of the individual pixels in the band, P is the total number of pixels in the band, FMS_p is the value of the pixel in the pan-sharpened band and $DsMS_p$ is the value of the pixel in the downsampled multispectral band. Once the *frRMSE* for each band has been obtained, the *frERGAS* index can be calculated (equation 2):

$$frERGAS = 100 \frac{r_{pan}}{r_{ms}} \sqrt{\frac{1}{N} \sum_{n=1}^N \frac{frRMSE_n^2}{DsMS_n^2}} \quad (2)$$

where r_{pan} is the spatial resolution of the panchromatic image, r_{ms} is the spatial resolution of the multispectral image, n refers to each of the multispectral bands involved in the pan-sharpening, N is the number of bands and $DsMS_n$ is the arithmetic mean of the downsampled multispectral band n .

The value of ERGAS shows a strong tendency to decrease when the quality of the pan-sharpened product increases. Values of less than 3 refer to an acceptable pan-sharpening quality (Wald, 2000; Ozdarici Ok and Akyurek, 2011), which improves as it approaches zero.

The ERGAS index in full resolution mode is necessary to check that there has not been a significant alteration of the radiometric values originally contained in the MS image. However, this is not sufficient on its own because if a new image was to be obtained just by artificially increasing the spatial resolution of the original image (without any pan-sharpening algorithm applied), its ERGAS value would be close to 0, which is the maximum possible. Therefore, other quality measures should be used.

Another way to apply the ERGAS index is to use the *reduced resolution* mode. This consists of 1) upscaling the MS image and the PAN image by applying an equivalent degradation of the spatial ratio, 2) performing the pan-sharpening with these new multispectral and panchromatic images, RMS and RPAN, respectively, and 3) comparing the result (FRMS) with the original multispectral image (MS) using the *rrERGAS* index, i.e. ERGAS in reduced resolution mode (equation 4). The *rrRMSE* would look like this (equation 3):

$$rrRMSE = \sqrt{\frac{1}{P} \sum_{p=1}^P (MS_p - FRMS_p)^2} \quad (3)$$

In addition, $rrERGAS$ is:

$$rrERGAS = 100 \frac{r_{ms}}{r_{ms}^2 / r_{pan}} \sqrt{\frac{1}{N} \sum_{n=1}^N \frac{rrRMSE_n^2}{MS_n^2}} \quad (4)$$

235 The interpretation of ERGAS in reduced resolution mode is the same as above. The main drawback of this approach is that it assumes that the RMS image is what the sensor would have observed if its spatial resolution were $\frac{r_{ms}^2}{r_{pan}}$ and that RPAN is what the sensor would have observed if its spatial resolution was r_{ms} . Something that normally can't be contrasted. The results of this analysis are sensitive to the method of spatial degradation of images. In our case a 5×5 Gaussian filter is applied to resample the MS and PAN images.

240 Since the ERGAS index only considers the spectral characteristics of the image, Lillo-Saavedra et al. (2005) proposed a new spatial index, called the spatial ERGAS index (equation 6), also introducing a spatial RMSE (equation 5).

$$spRMSE = \sqrt{\frac{1}{P} \sum_{p=1}^P (AdPAN_p - FMS_p)^2} \quad (5)$$

where $AdPAN_p$ is each of the pixels of the image obtained by adjusting the histogram of the original panchromatic image to the histogram of the downscaled multispectral band in question.

$$spERGAS = 100 \frac{r_{pan}}{r_{ms}} \sqrt{\frac{1}{N} \sum_{n=1}^N \frac{spRMSE_n^2}{MS_n^2}} \quad (6)$$

245 We also calculated the running times of the pan-sharpening algorithms in a laptop with an Intel Core i7 64-bit processor, 16 gb of RAM memory and Xubuntu 16.04 as OS.

A comparison of the fused images in R and proprietary software was also carried out (ERDAS Imagine 2011, hereinafter ERDAS and ENVI 4.7, hereinafter ENVI). To this end, the same pan-sharpening were carried out in the respective programs. As regards proprietary software, the HPF pan-sharpening algorithm was run in ERDAS and the PCA and GS algorithm in ENVI. However, the PCA algorithm of the IKONOS and Landsat 8 images was run with ERDAS, since the results of ENVI were completely anomalous and therefore impossible to compare. The anomalous results of the ENVI PCA algorithm and the IKONOS image are probably related (based on the experience of the authors) to the fact that the algorithm implementing the mathematical transformation obtains a negative first component, which, after the inverse transformation, produces NDs very different from those in the original image (Figure 3).
 255 Implementation of the same algorithm produced even stranger results with the Landsat 8 image, an image in which all pixels have the same value (8603, 8905 and 9071 for the red, green and blue bands, respectively). Since these

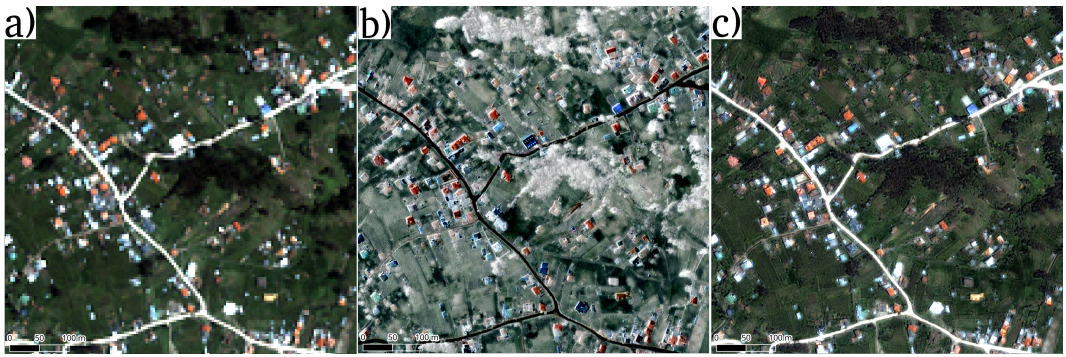


FIGURE 3 Clip of the IKONOS image showing some buildings and grassland near the city of Cuenca. (a) Original MS image; (b) PCA pan-sharpening implemented in proprietary software (ENVI); (c) PCA pan-sharpening implemented in R. This location can be visited in Google Earth by this [LINK](#).

programs gave consistent results for the pan-sharpening of the other images, it is considered that such anomalies may be associated with characteristics of the original images involved in the pan-sharpening.

260 HPF pan-sharpening in ERDAS only allows to use the central value options of the filtering matrix (see supplementary materials, subsection 2.1 High Pass Filter algorithm) when working with images with a ratio between 1.0 and 2.5. Therefore, for the images with ratios of 4 and 4.4 used in this work the default option was used.

On the other hand, to the best of our knowledge, there is no available commercial software that implements spectral and spatial ERGAS for evaluating the quality of image pan-sharpening, only the freely available software *IJFusion*¹.

265 Details of the R implementation of the two indices can be found in the supplementary materials.

2.4 | The fusionImage package

Despite the increasing use of pan-sharpening techniques in remote sensing and of R as a data analysis software, no R package implements such techniques and, to the best of our knowledge, only the *RStoolS* package (Leutner et al., 2019) implements PCA pan-sharpening. For this reason, we have created a new R package called *fusionImage* that includes three functions for image pan-sharpening and two functions to assess the quality of a pan-sharpening technique. All functions were programmed using R, so the package works indistinctly on Mac, Windows and GNU/Linux. Both the package, the manual and some test images are available in the supplementary materials. Updates of the package will be uploaded in <http://github.com/pacoalonso/fusionImage>. The package has been also submitted to CRAN, the R program repository.

275 3 | RESULTS AND DISCUSSION

With respect to the qualitative evaluation, all the pan-sharpened images are clearly more helpful for visual interpretation (Figure 4 to 13). The results presented in Table 2 show how a better qualitative evaluation is obtained in the images with higher spatial ratio between the MS image and the PAN image resolutions (QuickBird and IKONOS images

¹<http://ijfusion.es>

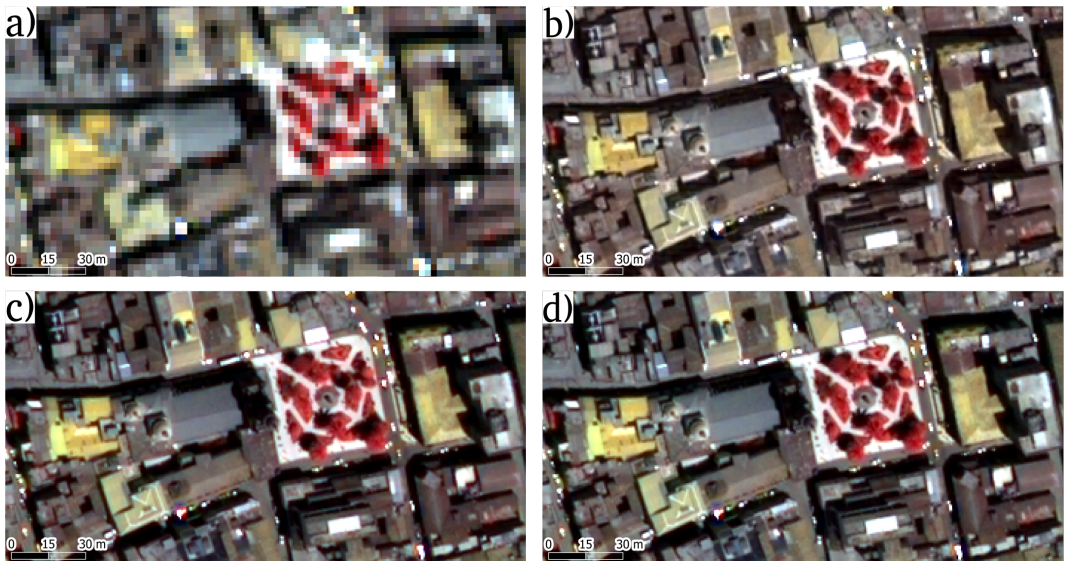


FIGURE 4 Clip of the QuickBird image showing the Cathedral of Azoges and Work Park. (a) Multi-spectral composite image; (b) HPF pan-sharpening; (c) PCA pan-sharpening and (d) GS pan-sharpening. This location can be visited in Google Earth by this [LINK](#).

with spatial resolution ratio of 4 and Natmur-08 with ratio of 4.4).

280 The high visual quality of the images with a spatial resolution ratio of 4 and 4.4 can be partly explained by the visual perception of the degree of improvement in the pan-sharpened images as the spatial ratio increases. This, however, raises the question as to how reliable the pan-sharpening between MS and PAN images would be at a larger spatial ratio (the present research uses images with ratios lower or equal than 4.4).

285 Landsat 7 and Landsat 8 images show greater colour distortion with the three pan-sharpening methods. In the case of Landsat 7 image, distortions are smaller when the HPF pan-sharpening is used (Figure 8 and 9); on the other hand, for the Landsat 8 image, the GS pan-sharpening produces the lowest distortion (Figure 10 and 11). The qualitative evaluation reveals better results for the QuickBird, IKONOS and Natmur-08 images, especially with HPF and GS, both in spectral and spatial terms.

290 With respect to the quantitative evaluation (Figure 14), the results show that no pan-sharpening method obtains optimal results simultaneously for all the images used. The best results for $frERGAS$ were obtained with HPF pan-sharpening in the QuickBird and Landsat 7 images, followed by GS pan-sharpening. This is important, considering that the HPF algorithm is based on map algebra operations, which makes its implementation simpler compared with other methodologies, and also consumes less time to obtain the merged bands (Table 3). However, in the case of Landsat 8 and Natmur-08 images, the results are much more even. As regards the GS pan-sharpening method, the simulated PAN band that is used as the first band for the Gram-Schmidt transformation was calculated as the average of all the MS bands used. However, it could be calculated by weighting the original MS bands based on the sensor calibration parameters, which, according to Laben and Brower (2000), could improve the pan-sharpening process, although few sensors provide the weighting coefficients. Some studies are even more conclusive and emphasise the most appropriate pan-sharpening method; however, such investigations evaluate just a certain type of image (sensor)
 295
 300 (Chavez et al., 1991; Nikolakopoulos, 2008), as opposed to the five types of images used in this research.

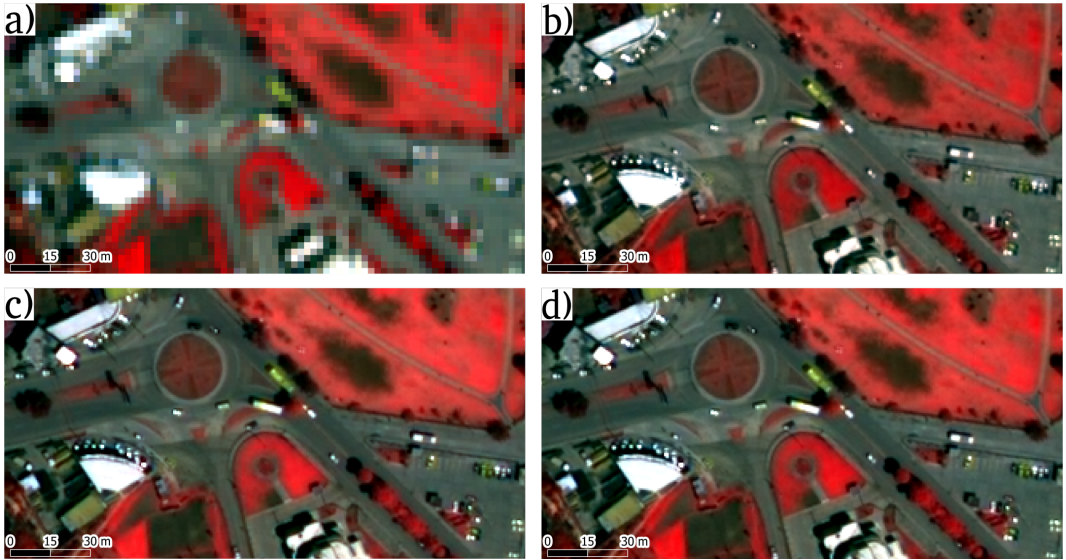


FIGURE 5 Clip of the QuickBird image showing a roundabout to access Azogues bus station. (a) Multi-spectral composite image; (b) HPF pan-sharpening; (c) PCA pan-sharpening and (d) GS pan-sharpening. This location can be visited in Google Earth by this [LINK](#).

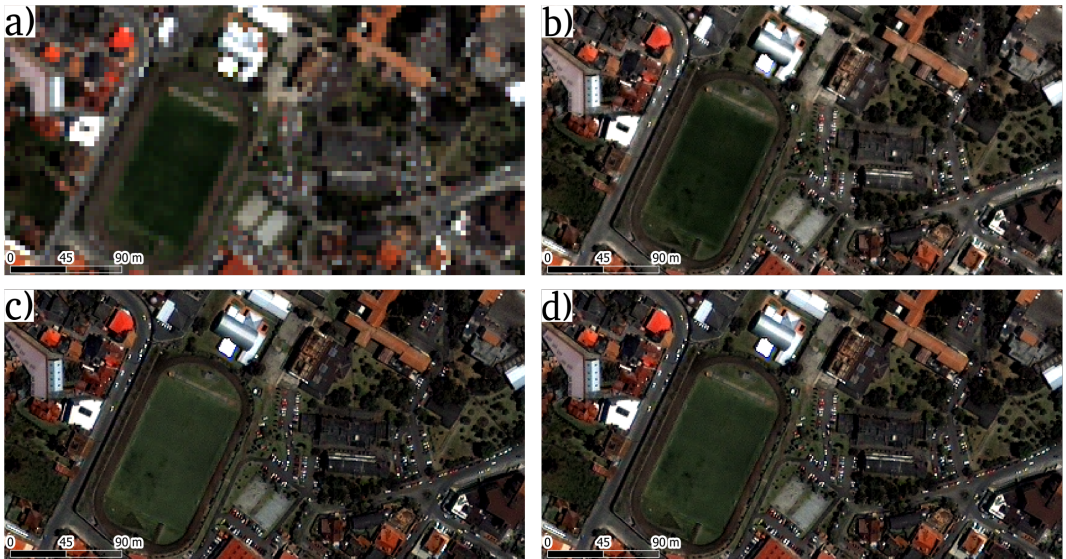


FIGURE 6 Clip of the IKONOS image showing the University of Cuenca campus. (a) Multi-spectral composite image; (b) HPF pan-sharpening; (c) PCA pan-sharpening and (d) GS pan-sharpening. This location can be visited in Google Earth by this [LINK](#).

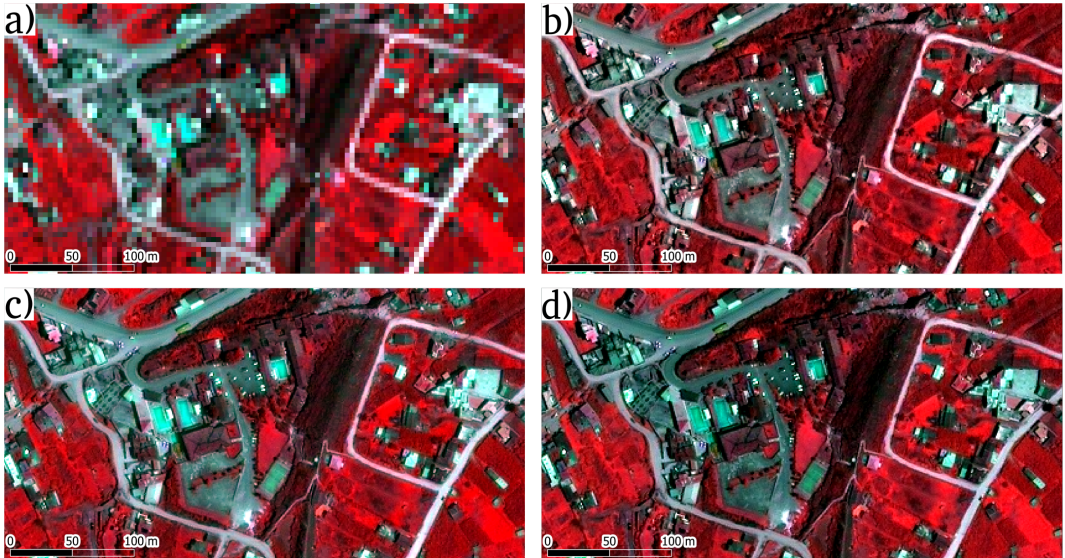


FIGURE 7 Clip of the IKONOS image showing Baños-Cuenca water pools. (a) Multi-spectral composite image; (b) HPF pan-sharpening; (c) PCA pan-sharpening and (d) GS pan-sharpening. This location can be visited in Google Earth by this [LINK](#).

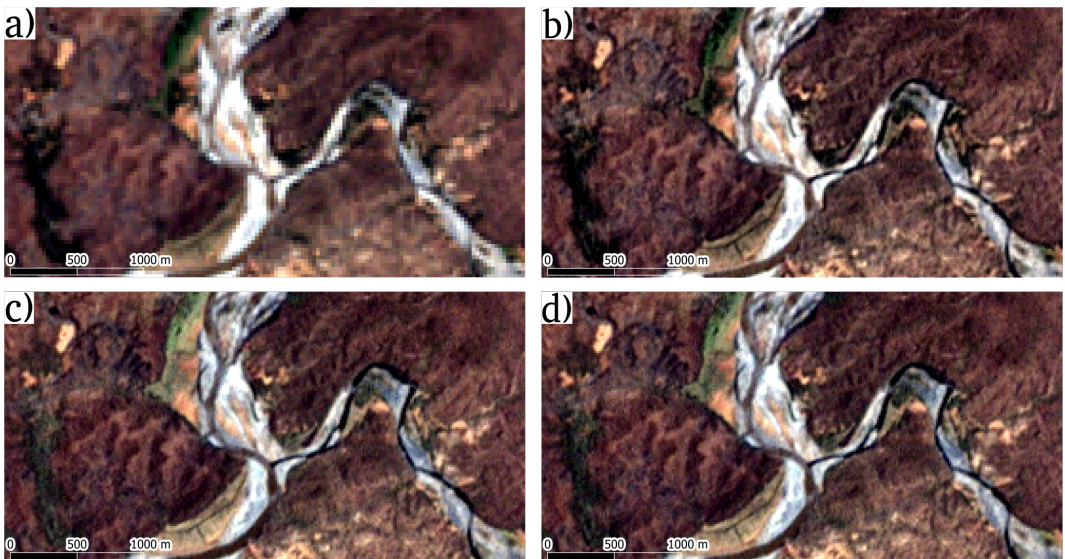


FIGURE 8 Clip of the Landsat 7 image showing a segment of the River Chira and one of its tributaries, 10 km downstream from Zapotillo. (a) Multi-spectral composite image; (b) HPF pan-sharpening; (c) PCA pan-sharpening and (d) GS pan-sharpening. This location can be visited in Google Earth by this [LINK](#).

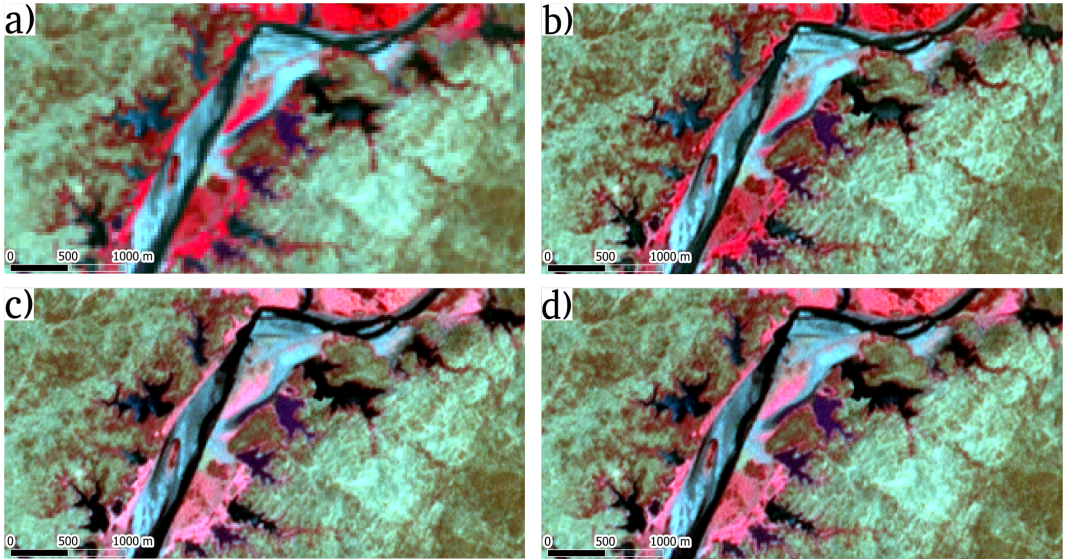


FIGURE 9 Clip of the Landsat 7 image showing the tail of the Poechos-Peru reservoir. (a) Multi-spectral composite image; (b) HPF pan-sharpening; (c) PCA pan-sharpening and (d) GS pan-sharpening. This location can be visited in Google Earth by this LINK.

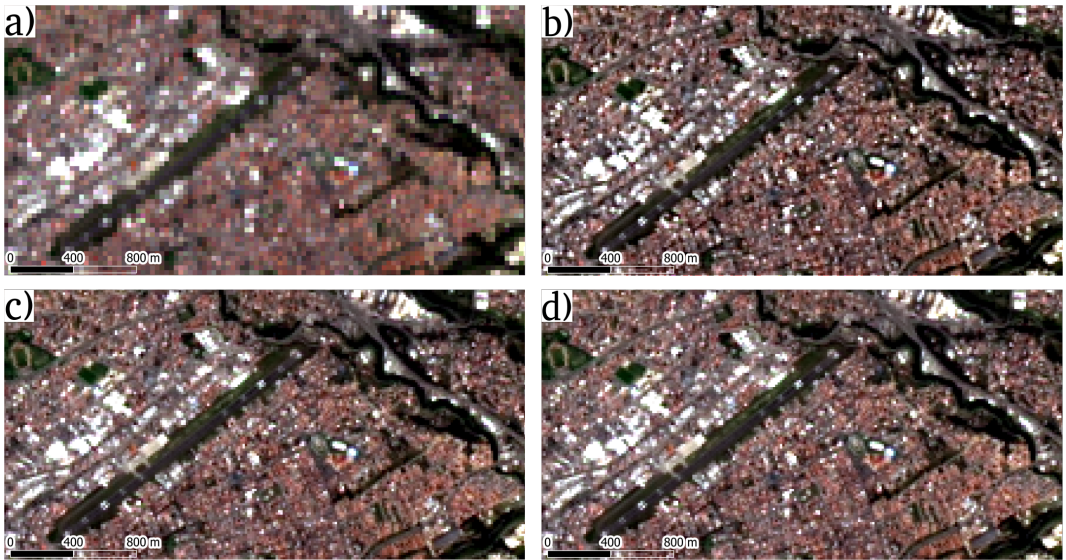


FIGURE 10 Clip of the Landsat 8 image showing the Mariscal La Mar Cuenca Airport. (a) Multi-spectral composite image; (b) HPF pan-sharpening; (c) PCA pan-sharpening and (d) GS pan-sharpening. This location can be visited in Google Earth by this LINK.

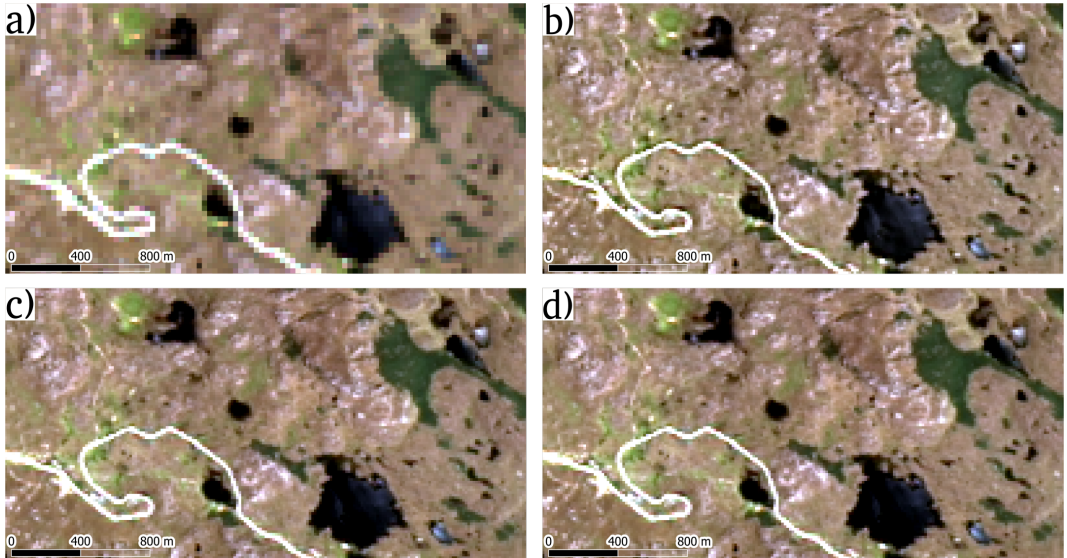


FIGURE 11 Clip of the Landsat 8 image showing the Cajas National Park, Toreadora lagoon and Cuenca-Guayaquil road. (a) Multi-spectral composite image; (b) HPF pan-sharpening; (c) PCA pan-sharpening and (d) GS pan-sharpening. This location can be visited in Google Earth by this [LINK](#).

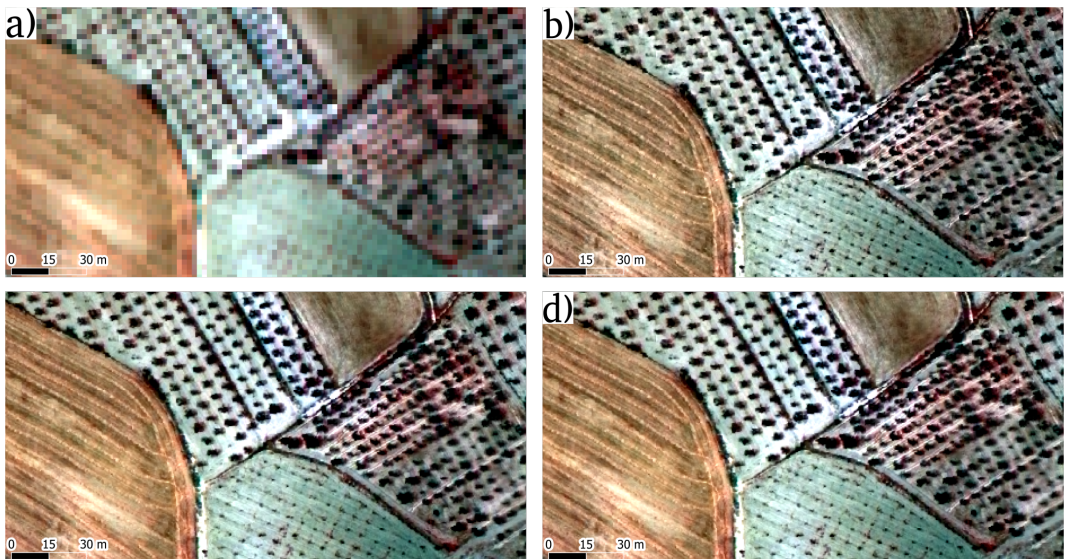


FIGURE 12 Clip of the Natmur-08 image showing agricultural plots in Archivel (Region of Murcia). (a) Multi-spectral composite image; (b) HPF pan-sharpening; (c) PCA pan-sharpening and (d) GS pan-sharpening. This location can be visited in Google Earth by this [LINK](#).

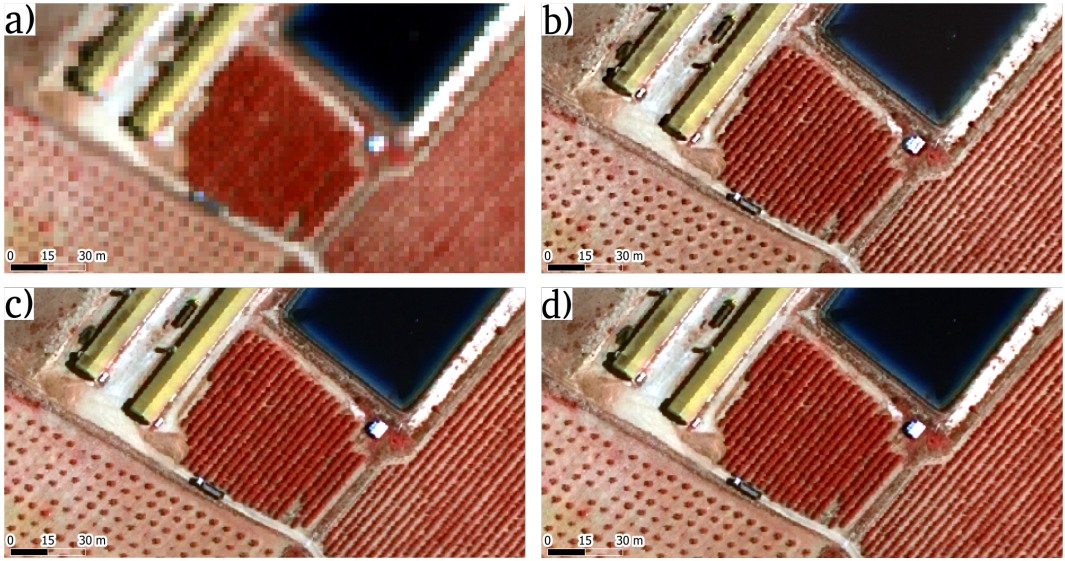


FIGURE 13 Clip of the Natmur-08 image showing edifications, irrigation pond and trees in Archivel (Region of Murcia). (a) Multi-spectral composite image; (b) HPF pan-sharpening; (c) PCA pan-sharpening and (d) GS pan-sharpening. This location can be visited in Google Earth by this LINK.

TABLE 2 Qualitative assessment according to spectral criteria (brightness and existence of anomalous colours) and spatial criteria (sharpness of the edges and spatial contrast between different elements of the scene) after visual interpretation of Fig. 4 to 13.

Image	Figure	Spectral criteria			Spatial criteria		
		HPF	PCA	GS	HPF	PCA	GS
Quickbird	Fig. 4	5	4	5	5	5	5
	Fig. 5	5	4	4	5	4	5
IKONOS	Fig. 6	5	4	5	5	5	5
	Fig. 7	5	5	5	4	5	5
Landsat 7	Fig. 8	4	3	3	4	4	4
	Fig. 9	5	4	4	4	4	4
Landsat 8	Fig. 10	4	4	5	5	5	5
	Fig. 11	4	4	5	5	5	5
Natmur-08	Fig. 12	5	4	5	5	5	5
	Fig. 13	5	5	5	5	5	5

1=very bad; 2=bad; 3=acceptable; 4=good; 5 =very good.

HPF: High Pass Filter pan-sharpening; PCA: Principal Components Analysis; GS: Gram-Schmidt.

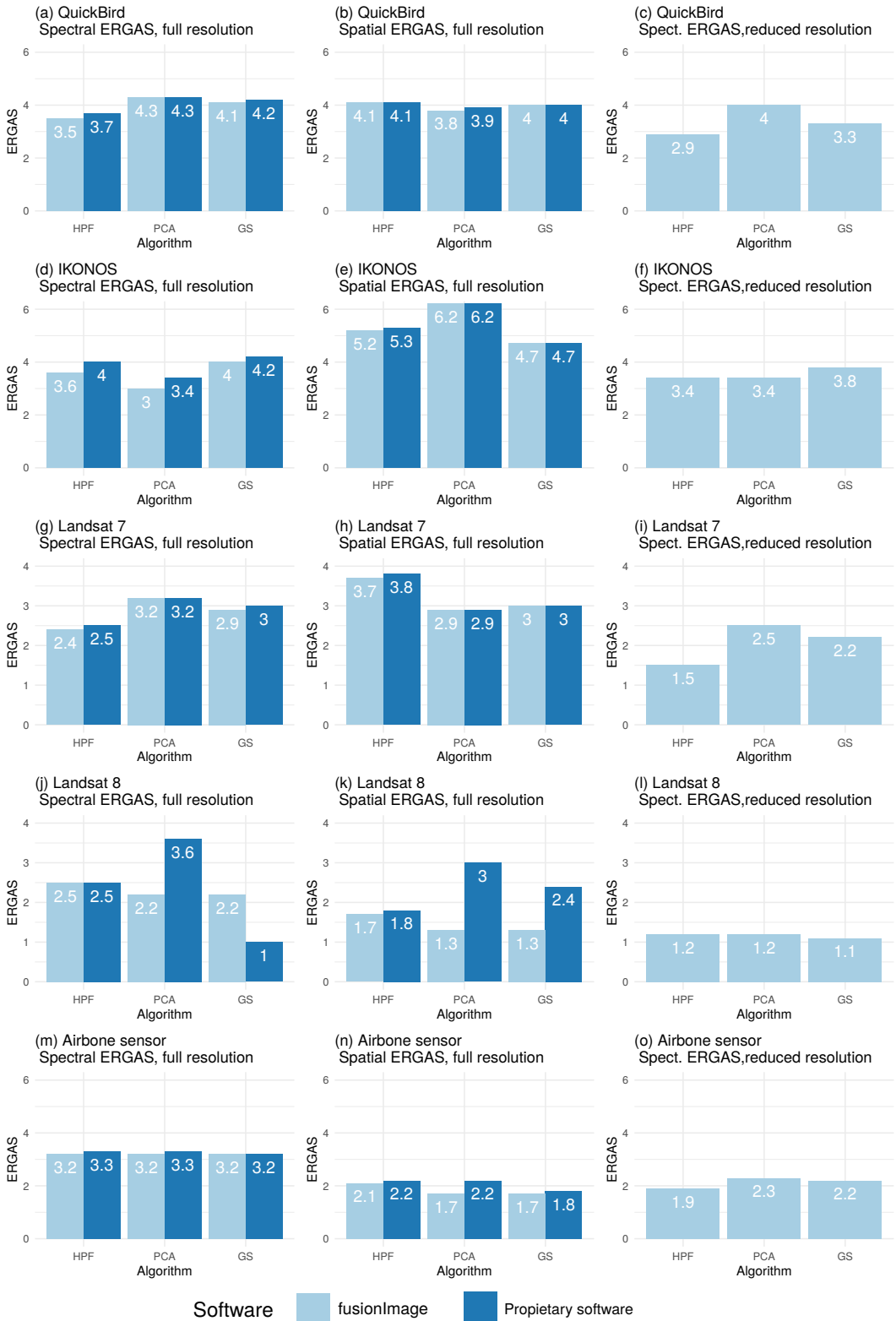


FIGURE 14 Quantitative assessment of the pan-sharpened images. HPF: High Pass Filter pan-sharpening; PCA: Principal Component Analysis; GS: Gram-Schmidt.

The ERGAS values obtained in reduced resolution mode ($rrERGAS$) are considerably lower than those obtained with full resolution mode, especially at low spatial ratios (Landsat 7 and 8). Also, there is sufficient coherence in terms of the results of ERGAS full resolution and ERGAS reduced resolution, the ranking of the pan-sharpening algorithms being similar in both modes.

305 Regarding the spatial ERGAS index, PCA pan-sharpening was the best option for QuickBird, Landsat 7 and Landsat 8 images, followed by GS. With respect to the comparatively low ratings obtained for the QuickBird and IKONOS images with the spatial ERGAS index in the three pan-sharpening methods, it should be noted that these two images share two characteristics: a high spatial ratio (4); and the presence of a high percentage of urban coverage. Xu et al. (2014) report that when these two conditions appear simultaneously, a spilling effect frequently occurs due to saturation of the signal during the acquisition phase of MS images as a result of the strong reflectance of some bright objects usually found in urban areas. In this case the fused image, for example those of QuickBird, would be wrongly evaluated in urban areas (as in our scene) and, in general, in areas with presence of bright objects. This may be the case of the Quickbird and IKONOS images used in our study.

315 Four out of the five types of image analysed show opposite results for the spatial and spectral ERGAS. Only in the case of Landsat-8 does the same algorithm (PCA) obtain better results in spectral and spatial ERGAS. It must be considered that the characteristics of the sensors and the spectral and spatial particularities of each analysed scene or image makes each algorithm respond differently in each case. This shows that it is not possible to identify any of the algorithms analysed in this research as the one that offers optimal results simultaneously in spectral and spatial terms. This would suggest the existence of a trade-off between the spectral and the spatial quality of the pan-sharpened images as suggested by Lillo-Saavedra and Gonzalo (2006), which would lend support to the idea of these authors that incorporating a parameter to modify this trade-off in pan-sharpening algorithms should be considered. In order to elaborate on possible explanations for the variation observed in the results when assessing spectral vs. spatial components, we believe that a different experimental design is needed. In our case, with the experiments carried out, we can only hypothesize possible causes. The literature in this field points to the effort needed to find the method that best meets the requirements and purposes of any research (Chen et al., 2008; Vivone et al., 2015). In conclusion, there are not better pan-sharpening algorithms, only better pan-sharpened images.

Figure 14 (c, f, i, l and o) shows the values of spectral and spatial ERGAS in full resolution mode when pan-sharpening is performed with proprietary software. With all the images and pan-sharpening algorithms, except Landsat 8 and GS, the spectral ERGAS values favour the implementation of R. The same can be said about spatial ERGAS. 320 It is difficult to offer a conclusive explanation since the source code of the proprietary software is not accessible. In the specific case of HPF, ERDAS only allows specific filters for images with a spatial ratio of less than 2.5. This could explain the differences in QuickBird, IKONOS and Natmur, but not in Landsat 7 and Landsat 8. The latter case must be analysed separately, especially taking into account the GS algorithm. Considering only $frERGAS$, it would seem that pan-sharpening with GS in ENVI obtains results ($frERGAS < 1$) that are much better than those obtained with 335 R. However, the spatial ERGAS produces the opposite results if it is compared with spectral ERGAS of GS with R, but in general terms it obtains a quite appropriate value (lower than 2.5). In this case it is necessary to visualize the resulting images (Figure 15), to see that pan-sharpening with proprietary software gave anomalous results, which led to a spurious increase in the spatial resolution without improving its interpretation capacity.

340 The performance of the pan-sharpening algorithms is presented in Table 3, which besides the processing time in seconds, presents a computation time indicator expressed in seconds per million pixels per band. According to this table and for the orders of magnitude of the size of the images, it can be claimed that the implementation of the HPF algorithm is the most efficient and the implementation of the GS algorithm, the least. When the number of pixels begins to increase, as in the case of the airborne sensor image, the computation time of the PCA algorithm greatly

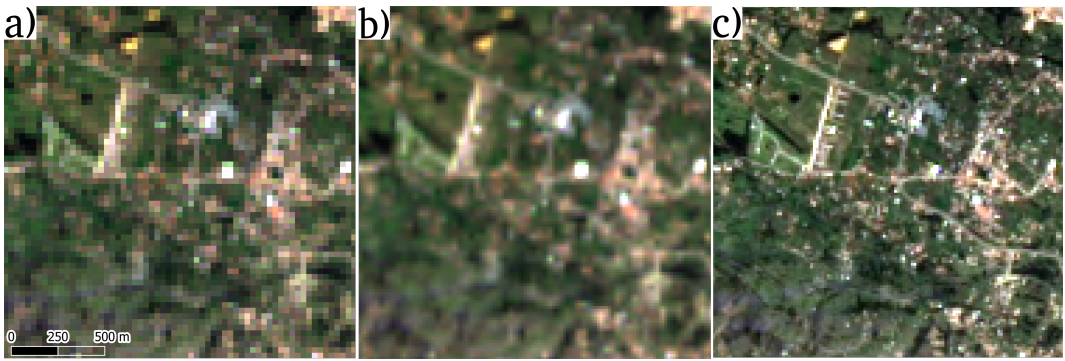


FIGURE 15 Clip of the Landsat 8 image showing buildings and grassland near the city of Cuenca. (a) Original image; (b) GS pan-sharpening implemented in proprietary software (ENVI); (c) GS pan-sharpening implemented in R. This location can be visited in Google Earth by this [LINK](#).

TABLE 3 Performance of the pan-sharpening algorithms implemented in the `fusionImage` package.

Platform	n° pixels per band (Millions)	n° bands	Seconds			Seconds/10 ⁶ pix. / band		
			HPF	PCA	GS	HPF	PCA	GS
QuickBird	12.9	4	35	39	57	0.68	0.7	1.11
IKONOS	32.4	4	82	114	130	0.63	0.88	1.01
Landsat 7	32.3	4	81	100	152	0.63	0.78	1.18
Landsat 8	11.1	3	19	22	33	0.58	0.66	0.98
Airborne sensor	45.8	4	131	431	184	0.72	2.35	1.01

HPF: High Pass Filter pan-sharpening; PCA: Principal Components Analysis pan-sharpening; GS: Gram-Schmidt pan-sharpening.

increases. This behaviour is striking, since in the case of IKONOS and Landsat 7 images, processing times increase from about 32 million pixels per band to much less competitive times (four times more) when processing 45.8 million pixels per band (airbone sensor). Taking into account the orders of magnitude considered, when the size of the images increases by 41.3 % the processing time increases more than 400 %.

4 | CONCLUSIONS

The objective of this study was threefold. First, to apply three pan-sharpening image techniques (High Pass Filter, Principal Component Analysis and Gram-Schmidt transformation) to fuse MS and PAN images obtained from four satellite platforms (QuickBird, IKONOS, Landsat 7 and Landsat 8) and an airborne platform with an Intergraph Z/I-Imaging Digital Mapping Camera in order to improve the spatial resolution of the original MS images. Second, to evaluate the results qualitatively by means of a visual comparison, and quantitatively based on two quality indices (the spectral and spatial ERGAS indexes). The last aim was to implement these techniques in the form of an open source program.

No qualitatively anomalous results were found in the images resulting from the algorithms implemented in R. However, visually anomalous results were obtained in specific cases when using other programs, as in the examples discussed (Figs. 3 and 15).

360 The qualitative evaluation of the results does not always agree with the quantitative evaluation. Therefore, each of these approaches can provide important analytical information and should be considered in a complementary way when assessing the quality of image pan-sharpening.

365 According to spectral ERGAS, HPF pan-sharpening offers better results for the QuickBird and Landsat 7 images, PCA for the IKONOS, Landsat 8 and airborne sensor. Although GS obtains appropriate results based on the quantitative evaluation, only once did it obtain the best score based on the spectral index (with Landsat 8 in reduced resolution mode). This contrast with the results obtained applying pan-sharpening algorithms with proprietary software, when GS obtained the best values with the spatial index in three of the five images analysed and was second best in the other two. However, with respect to the spatial ERGAS GS obtains the best results in three of the five images studied both in the R implementation and with proprietary software.

370 Any evaluation process has to be applied carefully since significant disagreements may arise if different methods are used. The results of this research indicate that there is a greater consistency when an independent evaluation is carried out for each image, not only because of the characteristics of the sensors themselves, but also because of the different terrain features and environmental factors that affect the images.

375 R is able to run both simple tasks and complex processes, while maintaining reliability and enabling the implementation of new algorithms such as those proposed in this study. The main problem with R is its limited capability to process large volumes of raster data, although in recent years significant progress has been made in this regard.

380 This research also offers some results about the computation times used in the processing of each image. This work offers results for images close to the actual application size, while in some previous works computation times are only provided for toy examples (very little images). The size of the images matters a lot in R and users of this language know that the computation times calculated for toy examples are of little use for extrapolation purposes, and that such computation times are only relevant when the architecture of the computer system is known and when images are processed close to the size of real applications. In this sense we have verified that when increasing the size of the images a threshold is reached at which computation times sharply increase, and that the efficiency of the PCA algorithm implementation is reduced considerably when a certain image size is surpassed (that could be around 35 x 4 million pixels). All this suggests that tools are needed in future versions of the package that allow images to be reduced to tiles before they are processed in parallel, and later joined to form a single image.

385 Geographers and most Earth, natural and social scientists, use data (remote sensing, sensor networks, observatory networks, territorial microdata, Big Data, etc.) in an intensive way, while open source software is increasingly used to manage these data (Alonso Sarría et al., 2012). In this respect, computer software has become a key element in research. However concern about the importance of the code has also led to a certain degree of mistrust of proprietary software. Some examples of which have been discussed in this work, but Barnes (2010) can also be cited. Rocchini and Neteler (2012) highlights the need to adopt a free software philosophy in Ecology, as Alonso Sarría et al. (2012) has done in Physical Geography and in this work we do for Geoinformatics.

395 The *fusionImage* package endows R, and so provides the GIS and Remote Sensing research community, with a new set of open source software tools. To the best of our knowledge, there is no open source multiplatform program that implements the three image pan-sharpening algorithms studied in this paper, so this contribution helps to reduce the gap in functionality that is only available in proprietary software.

ACKNOWLEDGEMENTS

The QuickBird image used in this work was provided by the Universidad de las Fuerzas Armadas (Ecuador). The IKONOS image from the city of Cuenca was facilitated by the Universidad del Azuay (Ecuador). The NatMur-08 image was provided by the CARM Environmental Integration and Management Service (Region of Murcia, Spain). We sincerely thank these three institutions for permission to use the images.

Fulgencio Cánovas-García thanks Gema González Romero and Juan Carlos Rodríguez Mateos from the University of Seville (Spain) for their help in several teaching activities. Without their help it would have been almost impossible to complete this work. We also thank the anonymous reviewers, whose suggestions have substantially improved the original manuscript.

CONFLICT OF INTREST

The authors declare no conflict of interest.

references

- Aiazzi, B., Baronti, S., Selva, M. and Alparone, L. (2006) Enhanced Gram-Schmidt Spectral Sharpening Based on Multivariate Regression of MS and Pan Data. 3806–3809.
- Alonso Sarria, F., Gomariz Castillo, F. and Cánovas García, F. (2012) Conocimiento abierto en Sistemas de Información Geográfica. Una estrategia para la Geografía física. *Nimbus. Revista de Climatología, Meteorología y Paisaje*, **29-30**, 21–34.
- Amro, I., Mateos, J., Vega, M., Molina, R. and Katsaggelos, A. K. (2011) A survey of classical methods and new trends in pansharpening of multispectral images. *EURASIP Journal on Advances in Signal Processing*, **2011**, 1–22.
- Barnes, N. (2010) Publish your computer code: it is good enough. *Nature*, **467**, 753.
- Basaeed, E., Bhaskar, H. and Al-Mualla, M. (2013) Comparative analysis of pan-sharpening techniques on DubaiSat-1 images. In *Information Fusion (FUSION), 2013 16th International Conference on*, 227–234.
- Belfiore, O. R., Meneghini, C., Parente, C. and Santamaria, R. (2016) Application of different pan-sharpening methods on worldview-3 images. *ARPN-JEAS*, **11**, 490–496.
- Bivand, R. S., Pebesma, E. J. and Gómez-Rubio, V. (2013) *Applied Spatial Data Analysis with R*. Springer, 2 edn.
- Brodu, N. (2017) Super-resolving multiresolution images with band-independent geometry of multispectral pixels. *IEEE Transactions on Geoscience and Remote Sensing*, **55**, 4610–4617.
- Chavez, P., Guptill, S. and Bowell, J. (1984) Image Processing Techniques for Thematic Mapper Data. In *50 th Annual ASP-ACSM Symposium*. Washington D.C.: American Society of Photogrammetry.
- Chavez, P., Stuart, C. and Anderson, J. (1991) Comparison of Three Different Methods to Merge Multiresolution and Multispectral Data: Landsat TM and SPOT Panchromatic. *Photogrammetric Engineering & Remote Sensing*, **57**, 295–303.
- Chen, S., Su, H., Zhang, R., Tian, J. and Yang, L. (2008) The tradeoff analysis for remote sensing image fusion using expanded spectral angle mapper. *Sensors*, **8**, 520–528.
- Chuvieco, E. (2016) *Fundamentals of Satellite Remote Sensing. An Environmental Approach*. CRC Press, 2 edn.
- Cliche, C., Bonn, F. and Teillet, P. (1985) Integration of the SPOT Panchromatic Channel into Its Multispectral Mode for Image Sharpness Enhancement. *Photogrammetric Engineering & Remote Sensing*, **51**, 311–316.

- Cánovas-García, F. and Alonso-Sarría, F. (2014) Comparación de técnicas de fusión en imágenes de alta resolución espacial. *GeoFocus*, **14**, 144–162.
- Darvishi Boloorani, A. (2008) *Remotely Sensed Data Fusion as a Basis for Environmental Studies: Concepts, Techniques and Applications*. Ph.D. thesis, Universität zu Göttingen.
- Digital Globe (2013a) IKONOS. Data Sheet. *Tech. rep.*
- (2013b) QuickBird. Data Sheet. *Tech. rep.*
- Du, Q., Younan, N., King, R. and Shah, V. (2007) On the Performance Evaluation of Pan-Sharpening Techniques. *IEEE Geoscience and Remote Sensing Letters*, **4**, 518–522.
- Duran, J. and Buades, A. (2019) Restoration of pansharpened images by conditional filtering in the PCA domain. *IEEE Geoscience and Remote Sensing Letters*, **16**, 442–446.
- Ehlers, M. and Astrand, P. J. (2008) Quality assessment for multi-sensor multi-date image fusion. *The International Archives of the Photogrammetry, Remote Sensing and Spatial Information Sciences*, 3797–3803.
- Ehlers, M., Jacobsen, K. and Schiewe, J. (2009) *ASPRS manual of GIS*, chap. High resolution image data and GIS, 721–777. American Society for Photogrammetry and Remote Sensing.
- Ehlers, M., Klonus, S., Astrand, P. and Rosso, P. (2010) Multi-sensor image fusion for pansharpening in remote sensing. *International Journal of Image and Data Fusion*, **1**, 25–45. URL: <http://www.tandfonline.com/doi/abs/10.1080/19479830903561985>.
- European Commission (1997) Corine Land Cover: Technical Guide.
- Ewertowski, M. W., Evans, D. J. A., Roberts, D. H. and Tomczyk, A. M. (2016) Glacial geomorphology of the terrestrial margins of the tidewater glacier, nordenskiöldbreen, svalbard. *Journal of Maps*, **12**, 476–487. URL: <https://doi.org/10.1080/17445647.2016.1192329>.
- Fonseca, L., Namikawa, L., Castejon, E., Carvalho, L., Pinho, C. and Pagamisse, A. (2011) Image fusion for remote sensing applications. In *Image fusion and its applications* (ed. Y. Zheng), 153–178. IntechOpen.
- Gangkofner, U. G., Pradhan, P. S. and Holcomb, D. W. (2008) Optimizing the High-Pass Filter Addition Technique for Image Fusion. *Photogrammetric Engineering & Remote Sensing*, **74**, 1107–1118.
- Gasparovic, M. and Jogun, T. (2018) The effect of fusing sentinel-2 bands on land-cover classification. *International Journal of Remote Sensing*.
- Ghosh, A. and Joshi, P. (2014) A comparison of selected classification algorithms for mapping bamboo patches in lower gangetic plains using very high resolution worldview 2 imagery. *International Journal of Applied Earth Observation and Geoinformation*, **26**, 298–311. URL: <http://www.sciencedirect.com/science/article/pii/S0303243413000974>.
- Gooslee, S. C. (2011) Analyzing remote sensing data in R: The landsat package. *Journal of Statistical Software*, **43**, 1–25. URL: <http://www.jstatsoft.org/v43/i04/>.
- Hengl, T., McMillan, B. A. and Wheeler, I. (2018) A brief introduction to open data, open source software and collective intelligence for environmental data creators and users. *PeerJ Preprints*, **6**.
- Hijmans, R. J. (2016) raster: Geographic data analysis and modeling.
- Huang, X., Wen, D., Li, J. and Qin, R. (2017) Multi-level monitoring of subtle urban changes for the megacities of china using high-resolution multi-view satellite imagery. *Remote Sensing of Environment*, **196**, 56–75. URL: <http://www.sciencedirect.com/science/article/pii/S0034425717301931>.

- Jagalingam, P. and Hegde, A. V. (2015) A review of quality metrics for fused image. *Aquatic Procedia*, **4**, 133–142.
- Jawak, S. D. and Luis, A. J. (2013) A comprehensive evaluation of pan-sharpening algorithms coupled with resampling methods for image synthesis of very high resolution remotely sensed satellite data. *Advances in Remote Sensing*, **2**, 332–344.
- Kaplan, G. (ed.) (2018) *Sentinel-2 Pan Sharpening-Comparative Analysis*, vol. 2 of *Multidisciplinary Digital Publishing Institute Proceedings*.
- Karathanassi, V., Kolokousis, P. and Ioannidou, S. (2007) A comparison study on fusion methods using evaluation indicators. *International Journal of Remote Sensing*, **28**, 2309–2341.
- Klonus, S. and Ehlers, M. (2009) Performance of evaluation methods in image fusion. In *12th International Conference on Information Fusion*, 1409–1416. Seattle, USA.
- Laben, C. and Brower, B. (2000) Process for Enhancing the Spatial Resolution of Multispectral Imagery Using Pan-Sharpener. *Tech. rep.*, United States Patent 6.011.875.
- Leutner, B., Horning, N. and Schwalb-Willmann, J. (2019) *RStoolbox: Tools for Remote Sensing Data Analysis*. URL: <https://CRAN.R-project.org/package=RStoolbox>. R package version 0.2.6.
- Lillo-Saavedra, M. and Gonzalo, C. (2006) Spectral or spatial quality for fused satellite imagery? a trade-off solution using the wavelet à trous algorithm. *International Journal of Remote Sensing*, **27**, 1453–1464.
- Lillo-Saavedra, M., Gonzalo, C., Arquero, A. and Martínez, E. (2005) Fusion of multispectral and panchromatic satellite sensor imagery based on tailored filtering in the Fourier domain. *International Journal of Remote Sensing*, **26**, 1263–1268.
- Liu, J. and Mason, P. (2009) *Essential Image Processing and GIS for Remote Sensing*. WILEY-BLACKWELL.
- Lu, J., Algazi, V. R. and Estes, R. R. (1996) Comparative study of wavelet image coders. *Optical Engineering*, **35**, 2605–2620.
- Maurer, T. (2013) How to Pan-Sharpen Images Using the Gram-Schmidt Pan-Sharpen Method - a Recipe. *ISPRS - International Archives of the Photogrammetry, Remote Sensing and Spatial Information Sciences*, **XL-1/W1**, 239–244.
- Nikolakopoulos, K. G. (2008) Comparison of Nine Fusion Techniques for Very High Resolution Data. *Photogrammetric Engineering & Remote Sensing*, **74**, 647–659. URL: <http://dx.doi.org/10.14358/PERS.74.5.647>.
- Ozdarici Ok, A. and Akyurek, Z. (2011) Evaluation of Image Fusion Methods on Agricultural Lands. *Journal of Earth Science and Engineering*, **1**, 107–113.
- Pebesma, E. (2018) Simple features for r: Standardized support for spatial vector data. *The R Journal*, **10**, 439–446.
- Pebesma, E., Nüst, D. and Bivand, R. (2012) The R Software Environment in Reproducible Geoscientific Research. *Eos*, **93**, 163–164.
- Pellemans, A. H. J. M., Jordans, R. W. L. and Allewn, R. (1993) Merging multispectral and panchromatic spot images with respect to the radiometric properties of the sensor. *Photogramm. Eng. Remote Sens.*, **59**, 81–87.
- Pohl, C. and Van Gendreen, J. (1998) Multisensor image fusion in remote sensing: concepts, methods and applications. *International Journal of Remote Sensing*, **19**, 823–854. URL: <http://www.tandfonline.com/doi/abs/10.1080/014311698215748>.
- R Development Core Team (2009) *R: A language and environment for statistical computing*. Vienna, Austria: R Foundation for Statistical Computing.
- Ranchin, T. and Wald, L. (2000) Fusion of High Spatial and Spectral Resolution Images: the ARSIS Concept and its Implementation. *Photogrammetric Engineering & Remote Sensing*, **66**, 49–61.
- Rocchini, D. and Neteler, M. (2012) Let the four freedoms paradigm apply to ecology. *Trends in Ecology & Evolution*, **27**, 310–311. URL: <http://dx.doi.org/10.1016/j.tree.2012.03.009>.

- Sarp, G. (2014) Spectral and spatial quality analysis of pan-sharpening algorithms: A case study in Istanbul. *European Journal of Remote Sensing*, **47**, 19–28. URL: doi:10.5721/EuJRS20144702.
- Schowengerdt, R. (1980) Reconstruction of Multispatial, Multispectral Image Data Using Spatial Frequency Content. *Photogrammetric Engineering & Remote Sensing*, **46**, 1325–1334.
- Shettigara, V. (1992) A Generalized Component Substitution Technique for Spatial Enhancement of Multispectral Images Using a Higher Resolution Data Set. *Photogrammetric Engineering & Remote Sensing*, **58**, 561–567.
- Shi, W., Zhu, C., Tian, Y. and Nichol, J. (2005) Wavelet-based image fusion and quality assessment. *International Journal of Applied Earth Observation and Geoinformation*, **6**, 241–251.
- Snehmani, Gore, A., Ganju, A., Kumar, S., Srivastava, P. K. and Ram R P, H. (2016) A comparative analysis of pansharpening techniques on quickbird and worldview-3 images. *Geocarto International*, **32**, 1268–1284.
- Vivone, G., Alparone, L., Chanussot, J., Dalla Mura, M., Garzelli, A., Licciardi, G. A., Restaino, R. and Wald, L. (2015) A critical comparison among pansharpening algorithms. *IEEE TRANSACTIONS ON GEOSCIENCE AND REMOTE SENSING*, **53**, 2565–2586.
- Wald, L. (2000) Quality of high resolution synthesised images: Is there a simple criterion? In *Fusion of Earth data: merging point measurements, raster maps and remotely sensed images*, 99–103. Sophia Antipolis, France: SEE/URISCA.
- (2002) *Data Fusion. Definitions and Architectures*, chap. Fusion of Images of Different Spatial Resolutions, 143–163. No. 8. Presses de l'Ecole, Ecole des Mines de Paris.
- Wald, L., Ranchin, T. and Mangolini, M. (1997) Fusion of Satellite Images of Different Spatial Resolutions: Assessing the Quality of Resulting Images. *Photogrammetric Engineering & Remote Sensing*, **63**, 691–699.
- Wang, Z., Ziou, D., Armenakis, C., Li, D. and Li, Q. (2005) A comparative analysis of image fusion methods. *IEEE transactions on geoscience and remote sensing*, **43**, 1391–1402.
- Xu, Q., Zhang, Y. and Li, B. (2014) Recent advances in pansharpening and key problems in applications. *International Journal of Image and Data Fusion*, **5**, 175–195. URL: <http://dx.doi.org/10.1080/19479832.2014.889227>.
- Yokoya, N., Grohnfeldt, C. and Chanussot, J. (2017) Hyperspectral and multispectral data fusion: A comparative review of the recent literature. *IEEE Geoscience and Remote Sensing Magazine*, **5**, 29–56.
- Yuhendra, H., Kuze, H. and Sri Sumantyo, J. (2010) Performance Analyzing of High Resolution Pan-Sharpener Techniques: Increasing Image Quality For Classification Using Supervised Kernel Support Vector Machine. *Selected Topics in Power Systems and Remote Sensing*, 260–268.
- Zhang, H. and Roy, D. (2016) Computationally inexpensive landsat 8 operational land imager (oli) pansharpening. *Remote Sensing*, **8**, 180.
- Zhang, Y. (2002) Problems in the Fusion of Commercial High-Resolution Satellites Images as well as LANDSAT 7 Images and Initial Solutions. Ottawa, Canada.
- (2004) Understanding image fusion. *Photogrammetric Engineering & Remote Sensing*, **70**, 657–661.
- (2008) Methods for Image Fusion Quality Assessment - A Review, Comparison and Analysis. *The International Archives of the Photogrammetry, Remote Sensing and Spatial Information Sciences*, **XXXVII**, 1101–1109.
- Zhang, Y. and Mishra, R. K. (2012) A review and comparison of commercially available pan-sharpening techniques for high resolution satellite image fusion. In *Geoscience and Remote Sensing Symposium (IGARSS)*, 182–185.
- Švab, A. and Oštir, K. (2006) High-resolution Image Fusion: Methods to Preserve Spectral and Spatial Resolution. *Photogrammetric Engineering & Remote Sensing*, **72**, 565–572.

A | DETAILED QUANTITATIVE ASSESSMENT OF THE PAN-SHARPENED IMAGES

TABLE 4 Detailed quantitative assessment of the pan-sharpened images. Values in bold indicate which method obtained the best result according to ERGAS.

Band	Spectral ERGAS			Spatial ERGAS			Spectral ERGAS			Spectral ERGAS			Spatial ERGAS		
	DsMS Vs FMS			AdPAN Vs FMS			MS Vs FRMS			DsMS Vs PrFMS			AdPAN Vs PrFMS		
	Full resolution			Full resolution			Reduced resolution			Full resolution			Full resolution		
QUICKBIRD															
	HPF	PCA	GS	HPF	PCA	GS	HPF	PCA	GS	HPF	PCA	GS	HPF	PCA	GS
1	3.04	3.85	3.59	3.69	2.63	3.05	2.57	3.61	3.02	3.21	3.87	3.72	3.75	2.70	3.04
2	3.43	4.55	4.25	3.62	2.03	2.63	2.84	4.03	3.33	3.66	4.58	4.39	3.69	2.09	2.61
3	4.36	5.68	5.30	4.57	3.12	3.84	3.47	4.95	4.04	4.60	5.64	5.41	4.66	3.22	3.83
4	3.02	2.27	2.55	4.23	6.09	5.77	2.78	3.06	2.71	3.23	2.66	2.75	4.32	6.12	5.78
Global	3.51	4.27	4.05	4.05	3.80	4.01	2.93	3.97	3.31	3.72	4.33	4.18	4.13	3.85	4.00
IKONOS															
	HPF	PCA	GS	HPF	PCA	GS	HPF	PCA	GS	HPF	PCA	GS	HPF	PCA	GS
1	5.08	3.95	5.66	7.61	9.21	6.35	4.92	4.85	5.41	5.70	4.63	6.00	7.77	9.28	6.32
2	3.44	2.97	4.07	4.49	5.43	3.31	3.06	3.07	3.51	3.83	3.29	4.24	4.59	5.48	3.29
3	2.73	2.03	2.95	4.25	5.10	3.59	2.66	2.62	2.95	3.16	2.42	3.16	4.34	5.13	3.57
4	2.79	2.73	2.51	3.31	3.59	4.84	2.48	2.46	2.41	2.68	2.95	2.84	3.41	3.52	4.83
Global	3.63	3.00	3.98	5.17	6.19	4.68	3.42	3.39	3.75	4.01	3.42	4.24	5.29	6.22	4.66
LANDSAT 7															
	HPF	PCA	GS	HPF	PCA	GS	HPF	PCA	GS	HPF	PCA	GS	HPF	PCA	GS
1	1.62	2.16	1.96	2.97	1.88	2.01	1.16	1.83	1.60	1.70	2.20	2.05	3.05	1.87	2.02
2	2.48	3.40	3.11	3.55	1.83	2.00	1.55	2.72	2.35	2.57	3.43	3.19	3.66	1.83	2.02
3	3.16	4.37	3.98	4.54	1.91	2.56	1.94	3.48	3.00	3.25	4.40	4.06	4.65	1.91	2.60
4	1.88	2.10	2.00	3.39	4.86	4.62	1.20	1.61	1.46	1.98	2.13	2.04	3.47	4.85	4.61
Global	2.36	3.15	2.89	3.66	2.92	3.00	1.50	2.52	2.19	2.45	3.18	2.96	3.75	2.92	3.01
LANDSAT 8															
	HPF	PCA	GS	HPF	PCA	GS	HPF	PCA	GS	HPF	PCA	GS	HPF	PCA	GS
1	2.26	1.97	1.99	1.68	1.39	1.33	1.16	1.02	0.99	2.30	3.25	0.79	1.83	2.80	2.49
2	2.37	2.08	2.11	1.38	1.02	1.00	1.20	1.15	1.12	2.42	3.44	0.92	1.57	2.80	2.21
3	2.71	2.39	2.42	1.85	1.54	1.62	1.31	1.33	1.29	2.78	3.94	1.15	2.03	3.36	2.53
Global	2.45	2.15	2.18	1.65	1.34	1.34	1.22	1.17	1.14	2.51	3.55	0.97	1.82	3.00	2.41
AIRBORNE SENSOR															
	HPF	PCA	GS	HPF	PCA	GS	HPF	PCA	GS	HPF	PCA	GS	HPF	PCA	GS
1	3.74	3.73	3.76	2.00	1.27	1.41	2.13	2.62	2.57	3.83	3.83	3.80	2.08	2.08	1.44
2	3.32	3.33	3.37	1.78	1.03	1.03	1.88	2.30	2.26	3.42	3.42	3.37	1.85	1.85	1.07
3	3.16	3.07	3.12	2.37	2.06	2.00	1.91	2.22	2.19	3.26	3.26	3.12	2.43	2.43	2.03
4	2.59	2.42	2.46	2.15	2.25	2.20	1.59	1.80	1.78	2.66	2.66	2.50	2.20	2.20	2.22
Global	3.23	3.17	3.21	2.09	1.73	1.72	1.89	2.25	2.22	3.32	3.32	3.23	2.15	2.15	1.75

ERGAS: *erreur relative globale adimensionnelle de synthèse*; HPF: High Pass Filter pan-sharpening; PCA: Principal Components Analysis; GS: Gram-Schmidt.

MS: Multispectral image; FMS: Fused Multispectral image; AdPAN: Adjusted Pachromatic image; FRMS: Fused-Reduced Multispectral image; PrFMS: Fused Multispectral image with proprietary software. Full resolution: same resolution as panchromatic image; Reduced resolution: same resolution as multispectral image.